

# RESONANCE EFFECTS IN THE OPTICAL ANTENNAS SHAPED AS FINITE COMB-LIKE GRATINGS OF NOBLE-METAL NANOSTRIPS

Olga V. Shapoval\*<sup>a</sup>, Alexander I. Nosich<sup>a</sup>, Jiří Čtyroký<sup>b</sup>

<sup>a</sup>Laboratory of Micro and Nano-Optics, Institute of Radio-Physics and Electronics of National Academy of Sciences of Ukraine, Proskury st. 12, Kharkiv 61085, Ukraine

<sup>b</sup>Institute of Photonics and Electronics AS CR, v.v.i., Chaberská 57, 18251 Prague 8, Czech Republic

## ABSTRACT

Active research into nanoscience and nanotechnologies that are available for nano fabrication have lead to considerable progress in the understanding of the optical properties of metals on nanometer scale. Here, noble-metal strip-like nanostructures are attractive objects of research. Indeed, they can be easily manufactured and serve as building blocks of optical nanoantennas and sensors with unique geometry-dependent optical properties. This is because they display intensive localized surface-plasmon resonances in the visible and far-infrared ranges that lead to near- and far-field enhancement effects. Thanks to surface-plasmon resonances, multi-element finite gratings have attractive properties of extraordinarily large reflection, absorption, and transmission, depending on the arrangement of the elementary cell of the grating. All these phenomena are greatly influenced by the so-called grating resonances which appear due to periodicity.

The 2D modeling of electromagnetic wave scattering by thin noble-metal nanosize strips and their finite-periodical ensembles arranged in comb-like gratings is considered. Our analysis is carried out using new efficient, convergent and accurate method. It is based, first, on the use of the generalized boundary conditions (GBC) valid for a thin and high-contrast material layer; they allow us to consider only the limit values of the field components and reduce integration contour to the collection of corresponding strip median lines. Second, for the building of discrete model of the obtained singular integral equations, we use very efficient Nystrom-type algorithm with quadrature formulas of interpolation type.

We study the SPRs of the finite periodic comb-like strip ensembles versus the incidence angle of the plane electromagnetic wave and the strip characteristics; both near-field and far-field properties of the associated surface-plasmon resonances and especially local field enhancements or focusing effects are analyzed. Moreover, we investigate the periodicity-induced properties such as the grating resonances in the context of the development of optimal design strategies for efficient multi-strip optical nanoantennas.

**Keywords:** noble-metal thin strips, nanoantennas, plasmons, grating resonances

## 1. INTRODUCTION

As active research into nanoscience and nanotechnology has been advancing rapidly in recent years [1-5], various methods have been developed to fabricate and theoretically model the optical properties of metals on nanometer scale.

The interest in these properties is associated with plasmon waves and plasmon resonances appearing on noble-metal nanostructures due to negative values of their dielectric functions [6]. They are promising for a variety of applications such as biosensing and efficient manipulation of light using the optical antennas in the visible and infrared ranges. Here, noble-metal strip-like nanostructures are attractive as fundamental objects, which are easily manufactured and serve as building blocks of nanoantennas and nanosensors with unique geometry-dependent optical properties.

Recently we have proposed a convergent, efficient, and accurate numerical algorithm to simulate electromagnetic wave scattering by stand-alone thin material strips and finite multi-strip ensembles [7]. Our mathematical simulation is

carried out, first, on the basis of GBCs valid for a thin and high-contrast material layer [8]; they allow us to consider only the limit values of the field components and reduce integration contours to the corresponding strip median lines. Second, for the building of discrete model of the obtained singular and hyper-singular IEs we use a very efficient Nystrom-type numerical algorithm with weighted quadrature formulas of interpolation type.

## 2. MATHEMATICAL SIMULATION

### 2.1 Problem Formulation

Consider the scattering of the H-polarized plane wave by a two-dimensional optical nanoantenna based on a comb-like finite nanostrip grating made of  $N$  identical silver strips. The corresponding freestanding geometry is shown in Fig. 1

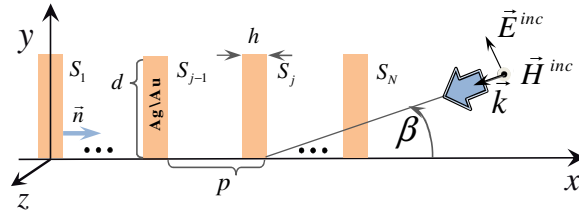


Figure 1. Cross-section of a free-standing comb-like finite nanostrip grating of  $N$  infinitely long (along  $z$ -axis) noble-metal strips.

The strips are assumed to be infinite along the  $z$ -axis, have thickness  $h$ , width  $d$  and form a grating with the period  $p$ . The silver is characterized with complex-valued permittivity  $\epsilon_r(\lambda)$  obtained via experimental data of [6], where  $\lambda$  is the free-space wavelength.

In the 2D scattering problem, one has to find a scalar function  $H_z^{sc}(\vec{r})$  that is the scattered magnetic field  $z$ -component. Here, the total magnetic field is a sum of the incident and scattered fields  $H_z(\vec{r}) = e^{-ik(x \cos \beta + y \sin \beta)} + H_z^{sc}(\vec{r})$ , where the latter field can be presented as a sum of single-layer and double-layer potentials

$$H_z^{sc}(\vec{r}) = k \sum_{j=1}^N \left[ \int_{S_j} v_j(\vec{r}') G(\vec{r}, \vec{r}') d\vec{r}' + \int_{S_j} w_j(\vec{r}') \frac{\partial G(\vec{r}, \vec{r}')}{\partial \vec{n}'} d\vec{r}' \right] \quad (1)$$

Here,  $k = 2\pi / \lambda$  is the free-space wavenumber,  $G(\vec{r}, \vec{r}') = (i/4)H_0^{(1)}(k|\vec{r} - \vec{r}'|)$  is the Green's function of the 2D Helmholtz equation, and unknown functions  $v_j(\vec{r})$  and  $w_j(\vec{r})$ ,  $j=1, \dots, N$  are the electric and the magnetic surface currents (jumps of the tangential components of  $H$  and  $E$  fields, respectively) induced on the strips i.e. at  $S_j = \{(x, y) : x \in [(j-1)p - h/2, (j-1)p + h/2], y \in [0, d]\}$ .

Exploiting the small thickness of each strip,  $h \ll \lambda$ , we assume it to be zero, i.e. we shrink their cross-sections to the set of median lines  $L_j = \{(x, y) : x = (j-1)p, y \in [0, d]\}$ . This enables us to neglect the internal fields inside the strips and impose the two-side GBCs at  $L = \bigcup_{j=1}^N L_j$ : (see [8] for more mathematical details),

$$\partial[H_z^+(\vec{r}) + H_z^-(\vec{r})] / \partial \vec{n} = -i2kR[H_z^+(\vec{r}) - H_z^-(\vec{r})], \quad (2)$$

$$[H_z^+(\vec{r}) + H_z^-(\vec{r})] = i2Qk^{-1} \partial[H_z^+(\vec{r}) - H_z^-(\vec{r})] / \partial \vec{n}. \quad (3)$$

Here, the coefficients  $R$  and  $Q$  are the so-called relative electric and magnetic resistivities (surface resistances),

$$R = i \cot(kh\sqrt{\epsilon_r}/2) / (2\sqrt{\epsilon_r}), \quad Q = (i/2)\sqrt{\epsilon_r} \cot(kh\sqrt{\epsilon_r}/2) \quad (4)$$

which contain the strip characteristics such as electric thickness  $kh$  and relative dielectric function  $\epsilon_r$ ,  $\vec{n}$  is the unit vector normal to the strip grating along the  $x$ -axis, and the superscripts  $\pm$  denote the limit values of the field at the top and bottom faces of the strip, respectively. These GBCs are valid if  $kh \ll 1$  and  $|\epsilon_r| \gg 1$  [7,8].

## 2.2 Singular and Hyper-Singular Integral Equations

By enforcing the GBC (2), (3) and using the properties of the limit values of potentials in (1), we obtain two coupled sets of IEs of the second kind for the unknown surface currents  $w_j(\vec{r})$  and  $v_j(\vec{r})$ , where  $\vec{r}_0, \vec{r} \in L$ ,

$$iQv_s(\vec{r}_0) + \sum_{j=1}^N \int_{L_j} w_j(\vec{r}) \frac{\partial G(\vec{r}, \vec{r}_0)}{\partial \vec{n}(\vec{r})} d\vec{r} + k \sum_{j=1}^N \int_{L_j} v_j(\vec{r}) G(\vec{r}, \vec{r}_0) d\vec{r} = -u_0(\vec{r}_0), \quad \vec{r}_0 \in L_s \quad (5)$$

$$ikRw_s(\vec{r}_0) + k \sum_{j=1}^N \int_{L_j} v_j(\vec{r}) \frac{\partial G(\vec{r}, \vec{r}_0)}{\partial \vec{n}(\vec{r}_0)} d\vec{r} + \sum_{j=1}^N \int_{L_j} w_j(\vec{r}) \frac{\partial G(\vec{r}, \vec{r}_0)}{\partial \vec{n}(\vec{r}_0) \partial \vec{n}(\vec{r})} d\vec{r} = -\partial u_0(\vec{r}_0) / \partial \vec{n}(\vec{r}_0), \quad \vec{r}_0 \in L_s \quad (6)$$

On changing the variables,  $y^j = d(t+1)/2$ ,  $x^j = (j-1)p$  and  $y_0^s = d(t_0+1)/2$ ,  $x_0^s = (s-1)p$ ,  $t, t_0 \in [-1, 1]$ , and introducing  $\rho_{js}^2(t, t_0) = (x^j - x_0^s)^2 + [y^j(t) - y_0^s(t_0)]^2 = (d/2)^2 [(t-t_0)^2 + \sigma_{js}^2]$ , where  $\kappa = kd/2$ ,  $\sigma_{js} = 2p(j-s)/d$ , the IEs can be rewritten in more detailed form,

$$4Q\kappa^{-1}v_s(t_0) + \sum_{j=1}^N \int_{-1}^1 v_j(t) K_v^{js}(\kappa, t, t_0) dt + \sum_{j=1}^N \int_{-1}^1 \tilde{w}_j(t) \sqrt{1-t^2} K_w^{js}(\kappa, t, t_0) dt = f_v^s(\kappa, t_0), \quad s=1, \dots, N, \quad (7)$$

$$4R\kappa^{-1}w_s(t_0) \sqrt{1-t_0^2} + \sum_{j=1}^N \int_{-1}^1 \tilde{w}_j(t) \sqrt{1-t^2} M_w^{js}(\kappa, t, t_0) dt + \sum_{j=1}^N \int_{-1}^1 v_j(t) M_v^{js}(\kappa, t, t_0) dt = f_w^s(\kappa, t_0), \quad s=1, \dots, N. \quad (8)$$

Note that the current-density functions  $v_j(t)$  are finite and non-zero at the endpoints  $[-1, 1]$ . The other currents  $w_j(t)$  are the functions which behave at the edges as  $w_j(t) = \tilde{w}_j(t)(1-t^2)^{1/2}$ , where  $\tilde{w}_j(t)$  are regular functions tending to finite limits at the endpoints. The right-hand parts are known regular functions for all  $\kappa$  and  $t \in [-1, 1]$  given by the following formulas, while  $n_p = d/p$ :

$$f_v^s(\kappa, t_0) = 4i\kappa^{-1} e^{-i\kappa(t_0+1)\sin\beta} e^{-2i\kappa(s-1)\cos\beta/n_p}, \quad f_w^s(\kappa, t_0) = 4\kappa^{-1} \cos\beta e^{-i\kappa(t_0+1)\sin\beta} e^{-2i\kappa(s-1)\cos\beta/n_p}. \quad (9)$$

Here, the kernel functions have the form,

$$K_v^{js}(\kappa, t, t_0) = \begin{cases} H_0^1(\kappa|t-t_0|), & j=s \\ H_0^1(k\rho_{js}(t, t_0)), & j \neq s \end{cases}, \quad K_w^{js}(\kappa, t, t_0) = \begin{cases} 0, & j=s \\ \sigma_{sj} \frac{H_1^1(k\rho_{js}(t, t_0))}{\rho_{js}(t, t_0)}, & j \neq s \end{cases} \quad (10)$$

$$M_v^{js}(\kappa, t, t_0) = \begin{cases} 0, & j=s \\ \sigma_{js} \frac{H_1^1(k\rho_{js}(t, t_0))}{\rho_{js}(t, t_0)}, & j \neq s \end{cases}, \quad M_w^{js}(\kappa, t, t_0) = \begin{cases} \frac{H_1^{(1)}(\kappa|t-t_0|)}{\kappa|t-t_0|}, & j=s \\ \sigma_{sj}^2 \frac{H_0^{(1)}(k\rho_{js}(t, t_0))}{\rho_{js}(t, t_0)^2} + \frac{H_1^{(1)}(k\rho_{js}(t, t_0))}{k\rho_{js}(t, t_0)} \frac{(t-t_0)^2 - \sigma_{sj}^2}{\rho_{js}(t, t_0)^2}, & j \neq s \end{cases} \quad (11)$$

The asymptotic behavior of the Hankel functions is  $H_0^{(1)}(z) \sim 2i \ln(z/2)/\pi$  and  $H_1^{(1)}(z)/z \sim (i/\pi) \ln z - 2i/(\pi z^2)$ ,  $z \rightarrow 0$ , respectively. Therefore it is only if the observation point coincides with the integration point ( $j=s$ ), that the kernel functions are singular.

### 2.3 Nystrom-type Discretization of IEs

Following [7,9], we isolate the singularities and discretize the resulted sets of IEs using Nystrom-type method with two different quadrature rules (but the same discretization order,  $n$ ) of interpolation type. For the integrals of IEs (8), (9) with unknown electric currents  $v_j(t)$ ,  $j=1, \dots, N$  we use the Gauss-Legendre quadrature formulas with nodes in the nulls of Legendre polynomials  $P_n(\tau_j) = 0$ ,  $j=1, \dots, n$  for the singular and regular parts, respectively,

$$\bullet \int_{-1}^1 v_j(\tau) \ln |\tau - \tau_{0i}| dt \approx \sum_{k=1}^n A_k S(\tau_k, \tau_{0i}) v_j(\tau_k), \quad (12)$$

$$\bullet \int_{-1}^1 v_j(\tau) R_v(\tau, \tau_{0i}) dt \approx \sum_{k=1}^n A_k v_j(\tau_k) R_v(\tau_k, \tau_{0i}), \quad (13)$$

where  $\tau_{0i} \in (-1,1)$  and weighted coefficients are given as,

$$A_k = 2 / [P_n'(\tau_k)^2 (1 - \tau_k^2)], \quad (14)$$

$$S(\tau, \tau_{0i}) = \frac{1}{2} \ln(1 - \tau_{0i}^2) + L_1(\tau_{0i}) + \sum_{l=1}^{n-1} P_l(\tau) [L_{l+1}(\tau_{0i}) - L_{l-1}(\tau_{0i})], \quad (15)$$

and  $L_l(t)$  is the Legendre function of the  $l$ -th order.

For the integrals of IEs (7), (8) with unknown magnetic currents  $\tilde{w}_j(t)$ ,  $j=1, \dots, N$  we use the Chebyshev quadrature formulas, with the weight  $(1-t^2)^{1/2}$ , with nodes in the nulls of Chebyshev polynomials of the second kind,  $t_j = \cos(\pi j / n)$ ,  $j=1, \dots, n$ . These formulas have the following form for the hyper-singular, log-singular and regular integrals meet in our analysis,

$$\bullet \int_{-1}^{+1} \tilde{w}_j(t) \ln |t - t_{0i}| \sqrt{1-t^2} dt \approx \sum_{k=1}^n \alpha_{ik} \tilde{w}_j(t_k) \quad (16)$$

$$\bullet \int_{-1}^{+1} \frac{\tilde{w}_j(t)}{(t - t_{0i})^2} \sqrt{1-t^2} dt \approx \sum_{k=1}^n \beta_{ik} \tilde{w}_j(t_k), \quad (17)$$

$$\bullet \int_{-1}^{+1} \tilde{w}_j(t) R_w(t, t_{0i}) \sqrt{1-t^2} dt \approx \frac{\pi}{n+1} \sum_{k=1}^n \tilde{w}_j(t_k) R_w(t_k, t_{0i}) (1-t_k^2) \quad (18)$$

where coefficients  $\alpha_{ik}$  and  $\beta_{ik}$  are given by formulas,

$$\alpha_{ik} = -\frac{\pi}{n+1} (1-t_k^2) \left[ \ln 2 + 2 \sum_{l=1}^n \frac{T_l(t_k) T_l(t_{0i})}{l} + \frac{(-1)^k}{n+1} T_{n+1}(t_{0i}) \right], \quad \beta_{ik} = \begin{cases} \frac{\pi}{n+1} \frac{(1-t_k^2)(1-(-1)^{k+i})}{(t_k - t_{0i})^2}, & i = k \\ -\frac{\pi(n+1)}{2}, & i \neq k \end{cases} \quad (19)$$

Here,  $R_v(t, t_0)$ ,  $R_w(t, t_0)$  can be arbitrary regular functions on the interval  $[-1,1]$ , and  $T_l(t)$  is the Chebyshev polynomial of the second kind.

As the collocation nodes, we choose the corresponding discretization nodes  $\{\tau_{0i}\}$  for the first set of IEs, and  $\{t_{0j}\}$  for the second one, respectively.

Applying the above presented quadrature formulas, we arrive at a set of matrix equations of the orders  $2nN$  for the values  $v_j(\tau_k)$  and  $\tilde{w}_j(t_k)$ , where  $j=1, \dots, N$  and  $k=1, \dots, n$ ,

$$\sum_{j=1}^N \sum_{k=1}^n v(\tau_k) A_{lk}^{js} + \tilde{w}(t_k) B_{lk}^{js} = f_v^s(\kappa, \tau_{0l}), \quad l = \overline{1, n} \quad (20)$$

$$\sum_{j=1}^N \sum_{k=1}^n v(\tau_k) C_{lk}^{js} + \tilde{w}(t_k) D_{lk}^{js} = f_w^s(\kappa, t_{0l}), \quad l = \overline{1, n}, \quad (21)$$

and the matrix coefficients are given by formulas,

$$A_{lk}^{js} = \begin{cases} (2i/\pi) A_k S(\tau_k, \tau_{0l}) + A_k N_v(\kappa, \tau_k, \tau_{0l}) + 4Q\kappa^{-1} \delta_{lk}, & j = s \\ A_k K_v^{js}(\kappa \rho(\tau_k, \tau_{0l})), & j \neq s \end{cases} \quad (22)$$

$$B_{lk}^{js} = \begin{cases} 0, & j = s \\ \pi(1-t_k^2) K_w^{js}(\kappa, t_k, \tau_{0l}) / (n+1), & j \neq s \end{cases}, \quad C_{lk}^{js} = \begin{cases} 0, & j = s \\ A_k M_v^{js}(\kappa, \tau_k, t_{0l}), & j \neq s \end{cases} \quad (23)$$

$$D_{lk}^{js} = \begin{cases} \frac{i}{\pi} \alpha_{lk} - \frac{2i}{\pi \kappa^2} \beta_{lk} + \frac{\pi}{n+1} N_w(\kappa, t_k, t_{0l})(1-t_k^2) + 4R\kappa^{-1} \sqrt{1-t_k^2} \delta_{lk}, & j = s \\ \pi(1-t_k^2) M_w^{js}(\kappa, t_k, t_{0l}) / (n+1), & j \neq s \end{cases} \quad (24)$$

while  $\delta_{lk}$  is the Kronecker delta, and regular functions  $N_{v(w)}(\kappa, \tau, \tau_0)$  are defined as,

$$N_v(\kappa, \tau, \tau_0) = H_0^{(1)}(\kappa |\tau - \tau_0|) - (2i/\pi) \ln |\tau - \tau_0|, \quad N_w(\kappa, \tau, \tau_0) = \frac{H_1^{(1)}(\kappa |\tau - \tau_0|)}{\kappa |\tau - \tau_0|} - \frac{i \ln |\tau - \tau_0|}{\pi} + \frac{2i}{\pi \kappa^2 |\tau - \tau_0|^2} \quad (25)$$

These finite-size matrix equations represent discrete model of our initial IEs (5) and (6). On solving them numerically we obtain approximate solution of IEs in the form of interpolation polynomials of the order  $n$  for each of the surface current densities.

The chosen quadrature formulas ensure rapid convergence of numerical solutions to the accurate ones if discretization order  $n \rightarrow \infty$ . Conservative estimation gives the rates of convergence as  $O(1/n)$ , although the actual rate is always faster [7,9].

### 3. NUMERICAL RESULTS AND DISCUSSION

In this paper we focus specifically on the details of the mathematical simulation of the comb-like nanostructure gratings. Besides of that, in this section we present some preliminary results on the plasmon-type and grating-type resonance effects of the associated comb-like nanostructure gratings and their dependence on the number of strips  $N$ .

To characterize the optical properties of considered gratings, we have computed the normalized total scattering cross-section (TSCS) and absorption cross-section (ACS) as a function of the wavelength in the visible range.

In Fig. 2, the normalized by  $2Nd$  scattering and absorption spectra are presented for the single strip ( $N = 1$ ) under the normal incidence ( $\beta = 0$ ) and for the gratings of  $N = 2, 5, 10$  and 20 identical silver strips of the width  $d = 300$  nm, thickness  $h = 50$  and period  $p = 500$  nm. Note that for the gratings the angle  $\beta = 0$  corresponds to the grazing incidence with respect to the plane of the grating.

As one can see, if the number of the strips gets larger, the surface plasmon resonances deform and became less pronounced in contrast to the coplanar silver strip gratings, while the grating resonances near  $\lambda = p$  become sharper.

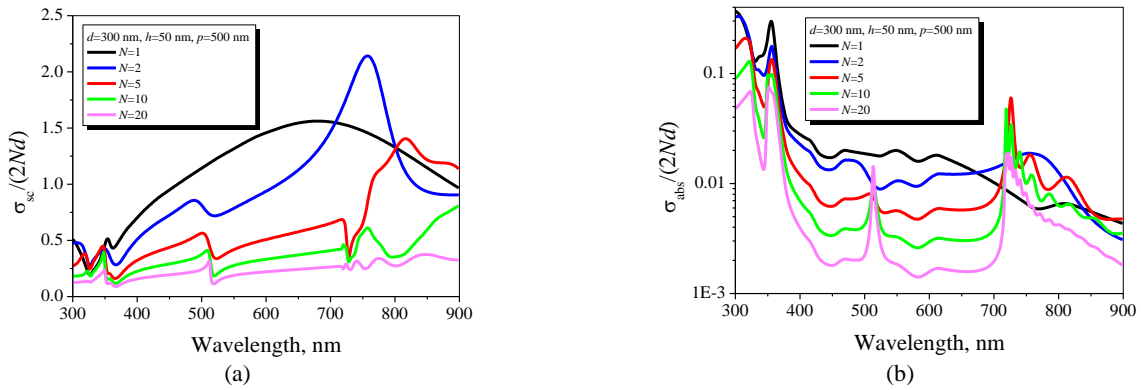


Figure 2. Normalized TSCS (a) and ACS (b) as a function of the wavelength for  $N = 1, 2, 5, 10$  and  $20$  silver strips of the width  $d = 300$  nm, thickness  $h = 10$  nm and period  $p = 500$  nm; the discretization order is  $n = 20$  ( $\beta = 0$ ).

To obtain better understanding of the resonance phenomena, we have investigated optical response of the two-strip resonator versus the strip width under the on-strip incidence. As one can see from Fig. 3 the strip width significantly affects the position of the plasmon resonances. Thus, wider strips lead to the red-shifting of the plasmon resonances, but the Q-factor keeps almost the same value.

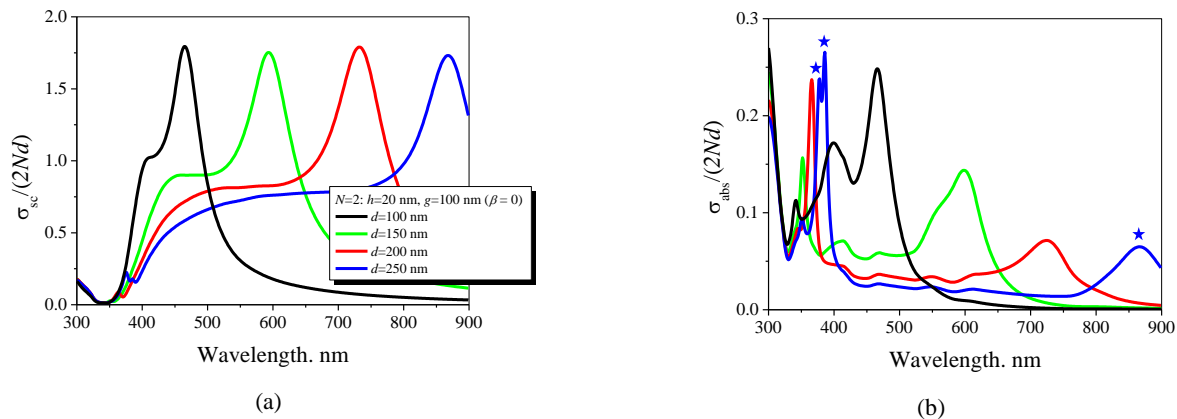


Figure 3. Normalized TSCS (a) and ACS (b) as a function of the wavelength for  $N = 2$  strips of the thickness  $h = 20$  nm and  $p = 100$  nm for the different values of the width  $d = 100, 150, 200$  and  $250$  under the edge-on ( $\beta = 0$ ) incident H-polarized plane wave.

In Fig. 4 we present the total near-field and the scattered far-field patterns for the two-strip resonator of  $d = 250$  nm,  $h = 20$  nm and  $p = 100$  nm at three resonance wavelengths  $\lambda = 377.64$  nm (a) and  $\lambda = 385.75$  nm (b) and  $\lambda = 868.01$  nm (c). Near-field distribution of such configuration shows strong interaction of light via the multiple reflections between the strips.

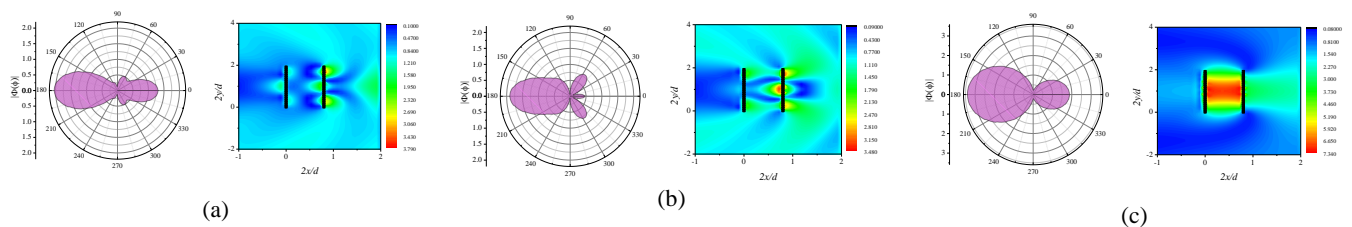


Figure 4. Scattered far-field and total magnetic near-field pattern at the wavelengths  $\lambda = 377.64$  nm (a),  $\lambda = 385.75$  nm (b) and  $\lambda = 868.01$  nm (c) for a two-strip resonator ( $N = 2$ ) of  $d = 250$  nm,  $h = 20$  nm and  $p = 100$  nm ( $\beta = 0$ ).

In the case of the grating consisting of dozens or even hundreds of strips, new effects appear induced by the existence of such a periodicity. In particular, the spectra of the scattering and absorption demonstrate the gradual build-up of the grating or lattice resonances near  $\lambda_G = p/m$ ,  $m = 1, 2, \dots$  (at normal incidence). This phenomena is explained by the specific poles of the field as a function of the wavelength that exist in the vicinities of Rayleigh anomalies of corresponding limit case of the infinite gratings.

In Fig. 5, the plots of the normalized TSCS and ACS versus the wavelength exhibit sharp grating resonances close to  $\lambda_G = p$  for the grating of as little number as of  $N = 20$  strips, in contrast to the coplanar strip gratings where similar grating resonance is observed only for the grating of  $N = 100$  strips [9]. It should be noted that if the number of elements in a finite grating gets larger, then the grating resonances become sharper and approach their limit forms valid for infinite gratings.

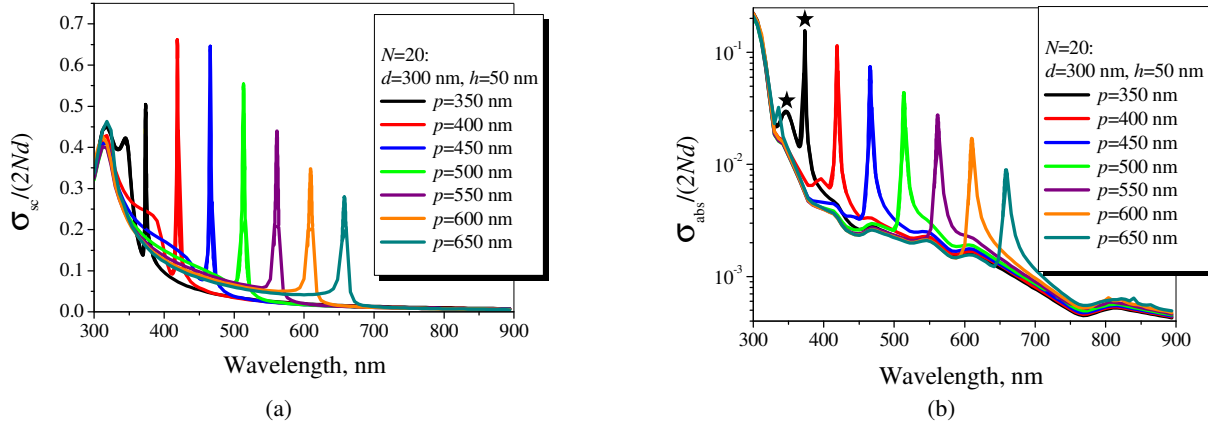


Figure 5. Normalized TSCS (a) and ACS (b) as a function of the wavelength for  $N = 20$  silver strips of  $d = 300$  nm and  $h = 50$  nm for the different values of the period  $p = 350, 400, 450, 500, 550, 600$  and  $650$  under the normally ( $\beta = \pi/2$ ) incident H-polarized plane wave.

As can be seen from Fig. 6 (b), the near-field pattern for the grating of  $N = 20$  strips of  $d = 300$  nm,  $h = 50$  nm and  $p = 350$  nm at the grating resonance wavelength  $\lambda_G = 373.55$  nm demonstrates field enhancement between strips with maximum magnitude of 10.4. This is in contrast to the near-field pattern in the plasmon resonance seen in Fig. 6 (a).

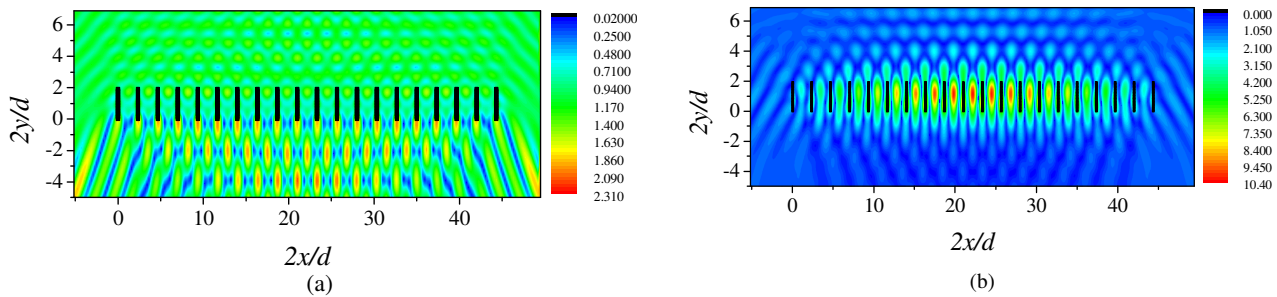


Figure 6. Total magnetic near-field pattern for the grating of  $N = 20$ ,  $d = 300$  nm,  $h = 50$  nm and  $p = 350$  nm at the plasmon resonance wavelength  $\lambda = 344.6$  nm (a) and at the grating resonance wavelength  $\lambda = 373.55$  nm (b).

#### 4. CONCLUSIONS

We have presented an efficient numerical method and the numerical results related to the accurate modeling of 2D electromagnetic wave scattering and absorption by optical nanoantennas shaped as comb-like metal strip gratings. The proposed Nystrom-type numerical analysis has been based on the median-line integral equations obtained using with the generalized boundary conditions and also on the quadrature formulas of interpolation type. Proposed algorithm is numerically efficient and guarantees fast convergence and controlled accuracy of computations. It allows simulating

fairly rapidly the scatterers consisting even of hundreds of nanosize noble-metal strips. In particular, we have investigated the interplay between the surface plasmon resonances and the grating or lattice resonances in the vicinities of the wavelengths of Rayleigh anomalies (i.e. caused by the periodicity), which depend on the number of strips in the grating.

## ACKNOWLEDGMENT

We thank Prof. J. Homola for encouragement and valuable discussions. Support of the National Academy of Sciences of Ukraine via the State Target Program “Nanotechnologies and Nanomaterials” and the European Science Foundation via RNP “Plasmon-Bionanosense” is acknowledged. The first author is also grateful to the International Visegrad Fund for the support in the form of Ph.D. scholarship.

## REFERENCES

- [1] G. Schider, J.R. Krenn, W. Gotschy, B. Lambrecht, H. Ditlbacher, A. Leitner, and F.R. Aussenegg, “Optical properties of Ag and Au nanowire gratings,” *J. Appl. Phys.*, vol. 90, no 8, pp. 3825-3830, 2001.
- [2] V. Giannini and J. A. Sánchez-Gil, “Calculations of light scattering from isolated and interacting metallic nanowires of arbitrary cross section by means of Green's theorem surface integral equations in parametric form,” *J. Opt. Soc. Am. A*, vol. 24, pp. 2822-2830, 2007.
- [3] T. Søndergaard, “Modeling of plasmonic nanostructures: Green's function integral equation methods,” *Phys. Stat. Sol. (b)*, vol. 244, pp. 3448-3462, 2007.
- [4] G. Della Valle, T. Søndergaard, and S. I. Bozhevolnyi, “Plasmon-polariton nano-strip resonators: from visible to infra-red,” *Opt. Exp.*, vol. 16, no 10, pp. 6867-6876, 2008.
- [5] M.R. Gadsdon, I.R. Hooper, and J.R. Sambles, “Optical resonances on sub-wavelength lamellar gratings,” *Opt. Exp.*, vol. 16, no 26, pp. 22003-22028, 2008.
- [6] P. B. Johnson and R. W. Christy, “Optical constants of the noble metals,” *Physical Review B*, vol. 6, pp. 4370-4379, 1972.
- [7] O. V. Shapoval, R. Sauleau, and A. I. Nosich. “Scattering and absorption of waves by flat material strips analyzed using generalized boundary conditions and Nystrom-type algorithm,” *IEEE Trans. Antennas Propag.*, vol. 59, no 9, pp. 3339-3346, 2011.
- [8] E. Bleszynski, M. Bleszynski, and T. Jaroszewicz, “Surface-integral equations for electromagnetic scattering from impenetrable and penetrable sheets,” *IEEE Antennas Propag. Mag.*, vol. 35, pp. 14-25, 1993.
- [9] O.V. Shapoval, R. Sauleau, A.I. Nosich, "Grating and plasmon resonances in the scattering of light by finite silver nanostrip gratings," *Int. J. Semicond. Physics, Quantum Electronics, Optoelectronics*, vol. 15, no 3, pp. 200-203, 2012.
- [10] O.V. Shapoval, R. Sauleau, A.I. Nosich, "Modeling of plasmon resonances of multiple flat noble-metal nanostrips with a median-line integral equation technique," *IEEE Trans. Nanotechnology*, vol. 12, pp. 442-449, 2013.